Computers and Structures 116 (2013) 35–49

Contents lists available at SciVerse ScienceDirect

Computers and Structures

journal homepage: www.elsevier.com/locate/compstruc

The finite element method enriched by interpolation covers

Jaehyung Kim, Klaus-Jürgen Bathe *

Department of Mechanical Engineering, Massachusetts Institute of Technology, Cambridge, MA 02139, USA

ARTICLE INFO

Article history:
Received 23 July 2012
Accepted 2 October 2012
Available online 14 November 2012

Keywords:
Enriched finite elements
3-node 2D & 4-node 3D elements
Cover functions
Higher convergence
Increase in accuracy
Adaptive interpolation

ABSTRACT

In this paper, we focus on an enriched finite element solution procedure for low-order elements based on the use of interpolation cover functions. We consider the 3-node triangular and 4-node tetrahedral displacement-based elements for two- and three-dimensional analyses, respectively. The standard finite element shape functions are used with interpolation cover functions over patches of elements to increase the convergence of the finite element scheme. The cover functions not only capture higher gradients of a field variable but also smooth out inter-element stress jumps. Since the order of the interpolations in the covers can vary, the method provides flexibility to use different covers for different patches and increases the solution accuracy without any local mesh refinement. As pointed out, the procedure can be derived from various general theoretical approaches and the basic theory has been presented earlier. We evaluate the effectiveness of the method, and illustrate the power of the scheme through the solution of various problems. The method also has potential for the development of error measures.

1. Introduction

Since the finite element method is frequently more robust and effective in the solution of problems compared to other methods, it has been widely used for the numerical analysis of solids, fluids, including heat transfer, and multi-physics problems. However, despite the success of the finite element method, there is still the burden that a good mesh for the analysis of a physical problem is needed. Indeed, in engineering practice, a substantial effort may be required to ensure that the mesh is fine enough in certain areas, but not too fine in other areas, and to achieve the desired solution accuracy may require that a problem be solved with a number of meshes. Also, in large deformation analyses, the mesh may need to be adapted during the incremental solution because distorted elements cause loss of accuracy and inhibit ideal convergence rates [1]. However, adaptive remeshing algorithms require projections of solutions from one mesh to another, which requires special procedures in order to avoid a significant loss in solution accuracy [2–6].

In order to develop more effective finite element methods, various approaches have been pursued. One approach is to use traditional finite element formulations with special enrichment functions, specific to the problem solved. This is a natural way to improve the effectiveness of finite element analysis, and first developments in that regard, for example, were published by Bathe et al. [7,8] and Bathe and Chaudhary [9] for the analysis of pipes and beams to incorporate ovalization and warping effects. Moes et al. [10], Belytschko and Black [11] and Daux et al. [12] incorporated enrichment functions to account for the presence of cracks, see also Ref. [13] and the references therein. Melenk and Babuška [14,15] presented the partition of unity finite element formulation to include Ansatz spaces containing the local properties of solutions, and Strouboulis et al. [16,17] used special handbook functions. However, these schemes focus on the more effective solution of specific problems and, mostly, do not apply to the solution of nonlinear problems.

In another approach to increase the effectiveness of the numerical solution, so-called meshless or meshfree methods have been developed. In particular, Belytschko et al. [18] proposed the element-free Galerkin technique, Liu et al. [19] developed the reproducing kernel particle method, Duarte and Oden [20] and Liszka et al. [21] presented the h-p cloud meshless method, Atluri and Zhu [22] proposed the meshless local Petrov–Galerkin method, and De and Bathe developed the method of finite spheres [23–26]. Additional meshless methods have been proposed, see for example Ref. [27]. A difficulty with all meshless techniques is the expense of the numerical integration. To improve upon the efficiency, Oñate et al. [28] developed a point collocation technique.

In another development, Shi [29–32] proposed the numerical manifold method, which combines the advantages of the classical finite element method and discontinuous deformation analysis techniques [33–35]. The procedure was also developed to enable the more effective analysis of problems with cracks and crack propagations [36–38].

The standard finite element method is a very effective technique for the solution of general physical problems since the numerical integration can be performed efficiently, the essential and natural boundary conditions can be easily imposed, and

* Corresponding author. Tel.: +1 6172536645.
E-mail address: kjb@mit.edu (K.J. Bathe).

0045-7949/$ - see front matter © 2012 Elsevier Ltd. All rights reserved.
http://dx.doi.org/10.1016/j.compstruc.2012.10.001

the global system matrix does not suffer from rank deficiency. Of course, for special problem solutions, effective special interpolation functions may be incorporated, see for example Refs. [7–17,39]. However, considering any proposed scheme, it is important that the procedure has no rank deficiency and is stable [1,40].

The objective in this paper is to focus on a scheme to increase the convergence of the traditional low-order finite element discretizations using 3-node triangular and 4-node tetrahedral elements in two- and three-dimensional analyses, respectively. The procedure uses the underlying finite element mesh enriched with interpolation covers over element patches to significantly increase the convergence rates of solutions, even when using distorted elements. While we focus on the specific details of the scheme, the theory of the procedure can be derived from and is closely related to the finite element methods discussed in Refs. [12,14,15], the numerical manifold method [41–47], the use of Taylor polynomials [48–50], and the schemes discussed in Refs. [51–53]. Indeed, the basic interpolations that we use have already been given in Ref. [52]. A particular difficulty discussed in these references is the linear dependency of the equations reached which is handled using special algorithms [52,53].

The contributions in our work are to show that, for the interpolation covers used on 3-node triangular 2D element and 4-node tetrahedral 3D element meshes, no rank deficiency is encountered – which we believe to be an important requirement in practical analyses – that the boundary conditions are best imposed as in the standard finite element method, and that, with the scheme used, a reasonably well-conditioned global coefficient matrix is obtained. We also illustrate how the method can be employed in adaptive interpolations, with different interpolation orders for different regions of the problem to be solved.

In Section 2, we give the finite element formulation enriched with interpolation cover functions. Thereafter, in Sections 3 and 4, we discuss the key theoretical and numerical aspects of our scheme regarding the stability, convergence and computational expense of the method. In Section 5, we present some illustrative solutions to demonstrate the proposed procedure, and finally, in Section 6, we give our concluding remarks.

2. Enriching finite elements by interpolation covers

Consider that a standard finite element mesh has been established for the solution of a physical problem. The accuracy in the solution sought is given by the kind of element and mesh used. To enrich the finite element procedure, we proceed as, it seems, earliest done in the numerical manifold method and define small sub-domains that overlap each other, where the common regions of the overlapped sub-domains are the finite elements in the given finite element mesh. Each sub-domain is covered by an interpolation cover, which allows for a higher-order interpolation of the solution sought and hence better solution accuracy. While in theory the approach has considerable generality, we focus on the enriched finite element interpolation for the use of three-node triangular finite elements in two-dimensional (2D) solutions, from which the 1D and 3D cases can directly be inferred. We consider the standard low-order finite elements because these are robust in linear and nonlinear solutions, but the major shortcoming is the solution accuracy obtained.

2.1. Functional approximation of a field variable

Let $Q^N := \{\underline{x}_i\}_{i=1}^N$ be a set of N given nodal points $\underline{x}_i = (x_i, y_i) \in \Omega$, and let $\{\mathcal{T}_h\} := \{\mathcal{E}^m\}_{m=1}^e$ be a family of e triangles generated by Q^N, which conforms to the domain Ω in which we seek the solution variable u

$$\bigcup_{m=1}^{e} \mathcal{E}^m = \Omega \tag{1}$$

without overlap, that is, $\mathcal{E}^j \bigcap \mathcal{E}^k = \varnothing$ for $j \neq k$. Fig. 1(a) shows the piecewise linear interpolation function h_i used in the solution. Let C_i be the support domain of h_i, i.e. $C_i = \mathrm{supp}(h_i),\ \forall i = 1, \ldots, N$, which we call the *cover region*. Hence the cover region C_i corresponds to the union of elements attached to the node i, see Fig. 1(b).

For each $\mathcal{E}^m$, let $i_c(m)$ be the set of cover indices defined by

$$i_c(m) := \left\{ i : C_i \bigcap \mathcal{E}^m \neq \varnothing \right\}. \tag{2}$$

For the 3-node triangular element, the overlapped region of the three cover regions C_i, C_j and C_k constitutes element m and hence $i_c(m) = \{i, j, k\}$, see Fig. 1(c). To now enrich the standard finite element interpolation for the solution of the variable u, we use interpolation cover functions, that is, over each cover region, we assign a set of *complete* polynomial bases. Let u_i be the usual nodal variable for the solution of u, then we use the polynomial bases of degree p over the cover region C_i given by

$$\mathcal{P}_i^p[u] = u_i + [\,\bar{x}_i \quad \bar{y}_i \quad \bar{x}_i^2 \quad \bar{x}_i\bar{y}_i \quad \bar{y}_i^2 \quad \cdots \quad \bar{y}_i^p\,]\underline{\tilde{a}}_i. \tag{3}$$

Here the coordinate variables $(\bar{x}_i, \bar{y}_i)$ are measured from node i (hence the subscript i does not denote a coordinate value but simply the node i at which the origin of the coordinate system $(\bar{x}_i, \bar{y}_i)$ is located, see Fig. 2). The vector $\underline{\tilde{a}}_i = [\,a_{i1} \quad a_{i2} \quad \cdots\,]^T$ lists additional degrees of freedom for the cover region C_i. Note that a normalization of the degrees of freedom can be introduced here, in that we may use $a_{ij}/\hat{h}$ corresponding to the linear terms and $a_{ij}/\hat{h}^2$ for the quadratic terms, etc., where $\hat{h}$ is a characteristic element length scale of the elements used in the mesh and the $\hat{h}$ terms are of course taken into the interpolation matrices. This approach is used in Refs. [52,53] proposing the same interpolations and in general improves the conditioning of the coefficient matrix (see Sections 3.2.1 and 4.1).

The enriched cover approximation of a field variable u is represented by

$$\mathcal{IC}^p[u] := \sum_{m=1}^{e} \sum_{i \in i_c(m)} h_i \mathcal{P}_i^p[u] = \sum_{m=1}^{e} \left(\sum_{i \in i_c(m)} h_i u_i + \sum_{i \in i_c(m)} \underline{\tilde{H}}_i \underline{\tilde{a}}_i \right) \tag{4}$$

where

$$\underline{\tilde{H}}_i = h_i [\,\bar{x}_i \quad \bar{y}_i \quad \bar{x}_i^2 \quad \bar{x}_i\bar{y}_i \quad \bar{y}_i^2 \quad \cdots \quad \bar{y}_i^p\,]. \tag{5}$$

Of course, if $\mathcal{P}_i^0[u] = u_i,\ \forall i$ is adopted, then the scheme reduces to the standard linear finite element interpolation. Indeed, as seen in Eq. (4), we can regard the enriched interpolation as the standard finite element interpolation *plus* additional higher order terms. While these terms can be derived in various ways by the approaches mentioned in Section 1, it is our objective here to focus on these enriched interpolations and evaluate how they perform in analyses.

To obtain some insight into the approach used, we can evaluate the coefficients in Eq. (3) at node i by taking partial derivatives of the interpolation cover function $\mathcal{P}_i^p[u]$ with respect to the nodal coordinate variables. Assuming that a complete set of polynomial bases of degree p is used, letting $u_i \equiv a_{i0}$ and assigning the subscript k to refer to the set of coefficients used, we can determine the coefficients by

$$\{a_{ik}\}_{k=0}^{k=(p+1)(p+2)/2-1} = \left\{ \frac{1}{\xi!\eta!} \frac{\partial^{(\xi+\eta)} \mathcal{P}_i^p[u]}{\partial \bar{x}_i^\xi \partial \bar{y}_i^\eta} \bigg|_{(\bar{x}_i, \bar{y}_i) = (0,0)} \right\}_{\xi+\eta=0}^{\xi+\eta=p} \tag{6}$$

where ξ and η are integers such that $0 \leqslant \xi,\ \eta \leqslant p$ and for $\xi = 0$ and $\eta = 0$, respectively, no derivative is taken. Now using $\bar{x}_j = x - x_j$ and $\bar{y}_j = y - y_j$, we can interpret the enriched interpolation in the

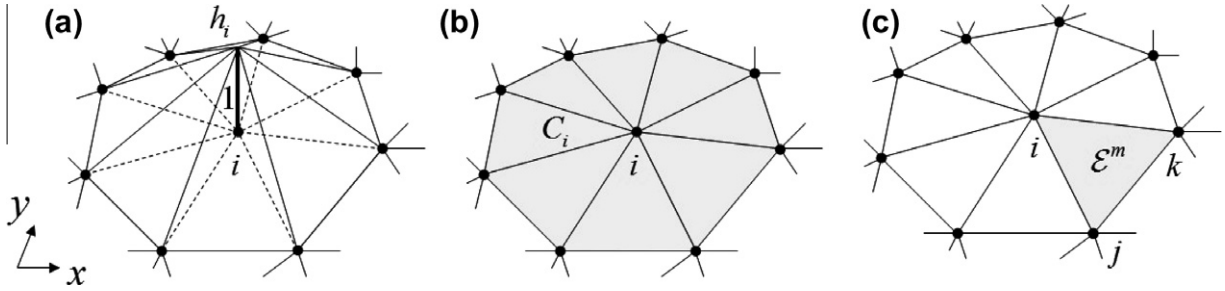

Fig. 1. Description of sub-domains for enriched cover interpolations: (a) usual linear nodal shape function, (b) cover region or elements affected by the interpolation cover, and (c) an element.

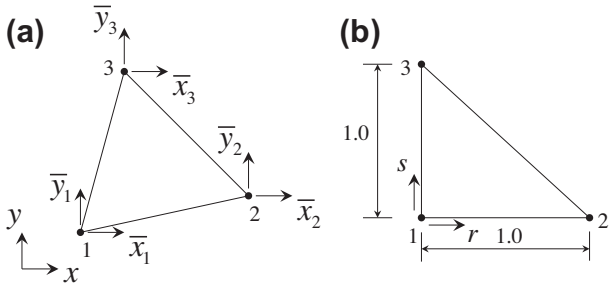

Fig. 2. Coordinate systems for a three-node triangular element: (a) global system (x,y) and nodal local coordinate systems $(\bar{x}_i, \bar{y}_i)$, $i = 1,2,3$, and (b) isoparametric coordinate system.

triangular element as a linear interpolation (or weighting) of three associated cover functions that are defined by Taylor polynomials expanded along each cover coordinate variable. This interpolation spans higher spatial bases than the standard finite element interpolation.

The use of the local coordinate systems $(\bar{x}_i, \bar{y}_i)$ is important compared to the use of global coordinates (x,y) as employed in Refs. [41–46,51], in that, firstly, the matrix conditioning is improved and, secondly, the nodal value u_i is separated from the additional degrees of freedom. Note that the essential boundary conditions can be directly imposed on u_i by also enforcing $\underline{\tilde{a}}_i = \underline{0}$. This treatment is indeed a necessary condition in order to avoid a rank deficient global matrix, see Section 3.1.

It should be emphasized that the cover interpolations can be different in different cover regions. For example, the cover interpolation for node i in Fig. 1(c) can be of different degree than the other cover functions for nodes j and k, and vice versa. This fact can be naturally used in an adaptive interpolation scheme without remeshing, as we shall illustrate in example solutions, see Section 5.

2.2. On the use of interpolation covers

An arbitrary degree of polynomial bases can be adopted in the cover interpolations. However, since high-order covers yield more unknowns (and, as we shall see, larger condition numbers of the stiffness matrices), we shall use up to quadratic covers in this work, i.e. we shall use $p \leqslant 2$.

For field variables u and v in $\Omega(\mathbb{R}^2)$, the enriched interpolations over a 3-node triangular element m given by Eq. (4) are

$$u_h^{(m)} = \sum_{i\in i_c(m)} \left(h_i u_i + \underline{\tilde{H}}_i \underline{\tilde{a}}_i^u \right), \quad v_h^{(m)} = \sum_{i\in i_c(m)} \left(h_i v_i + \underline{\tilde{H}}_i \underline{\tilde{a}}_i^v \right) \tag{7}$$

where u_i and v_i are the usual nodal values, and the $\underline{\tilde{a}}_i^u$ and $\underline{\tilde{a}}_i^v$ are vectors of unknown coefficients.

For linear covers, we have

$$\underline{\tilde{H}}_i = h_i[\bar{x}_i \quad \bar{y}_i] \tag{8}$$

and for quadratic covers we have

$$\underline{\tilde{H}}_i = h_i[\bar{x}_i \quad \bar{y}_i \quad \bar{x}_i^2 \quad \bar{x}_i\bar{y}_i \quad \bar{y}_i^2]. \tag{9}$$

Using properly arranged unknowns in vectors, the enriched interpolations $u_h^{(m)}$ and $v_h^{(m)}$ in matrix form become

$$\begin{bmatrix} u_h^{(m)} \\ v_h^{(m)} \end{bmatrix} = \begin{bmatrix} \underline{H}^{(m)} & \underline{\tilde{H}}^{(m)} & \underline{0} & \underline{0} \\ \underline{0} & \underline{0} & \underline{H}^{(m)} & \underline{\tilde{H}}^{(m)} \end{bmatrix} \begin{bmatrix} \underline{u} \\ \underline{\tilde{a}}_u \\ \underline{v} \\ \underline{\tilde{a}}_v \end{bmatrix} \tag{10}$$

in which $\underline{H}^{(m)}$ is the classical finite element interpolation matrix and $\underline{\tilde{H}}^{(m)} = [\underline{\tilde{H}}_1 \quad \underline{\tilde{H}}_2 \quad \underline{\tilde{H}}_3]$, where the element local subscripts (1,2,3) correspond to the global covers (i,j,k) in Fig. 1. Applying the usual differentiation rules, we have

$$\begin{bmatrix} u_{h,x}^{(m)} \\ u_{h,y}^{(m)} \end{bmatrix} = \begin{bmatrix} \underline{H}_{,x}^{(m)} & \underline{\tilde{H}}_{,x}^{(m)} \\ \underline{H}_{,y}^{(m)} & \underline{\tilde{H}}_{,y}^{(m)} \end{bmatrix} \begin{bmatrix} \underline{u} \\ \underline{\tilde{a}}_u \end{bmatrix}, \quad \begin{bmatrix} v_{h,x}^{(m)} \\ v_{h,y}^{(m)} \end{bmatrix} = \begin{bmatrix} \underline{H}_{,x}^{(m)} & \underline{\tilde{H}}_{,x}^{(m)} \\ \underline{H}_{,y}^{(m)} & \underline{\tilde{H}}_{,y}^{(m)} \end{bmatrix} \begin{bmatrix} \underline{v} \\ \underline{\tilde{a}}_v \end{bmatrix} \tag{11}$$

with

$$\begin{bmatrix} \underline{H}_{,x}^{(m)} & \underline{\tilde{H}}_{,x}^{(m)} \\ \underline{H}_{,y}^{(m)} & \underline{\tilde{H}}_{,y}^{(m)} \end{bmatrix} = \mathbf{J}^{-1} \begin{bmatrix} \underline{H}_{,r}^{(m)} & \underline{\tilde{H}}_{,r}^{(m)} \\ \underline{H}_{,s}^{(m)} & \underline{\tilde{H}}_{,s}^{(m)} \end{bmatrix} \tag{12}$$

where $\mathbf{J}$ is the Jacobian of the element [1], evaluated for each element without high-order coefficients.

In addition, the scheme can handle interpolations that have different polynomial degrees in different cover regions while keeping the same mesh structure. To define such *mixed (or adaptive)* interpolation schemes, we modify the interpolation operator used in Eq. (4) to

$$\mathcal{IC}^{\{ad\}}[u] := \sum_{m=1}^{e} \sum_{i\in i_c(m)} h_i \mathcal{P}_i^{p(i)}[u] \tag{13}$$

where $\{ad\}$ denotes the set of covers used and $p(i)$ denotes that p now depends on the node i. For example, if only linear and quadratic covers are adopted, then our scheme is given by $\mathcal{IC}^{\{1,2\}}[u]$. Note that the cover series $\{ad\}$ is user-defined but where the different cover interpolations shall be used in the mesh may either be user-defined or automatically established in an iterative scheme. In Section 5, we present some experiences with mixed order covers.

2.3. Governing equations in linear elastic solid mechanics

The principle of virtual work is of course directly applicable for our enriched finite element method [1], and is given by

$$\int_\Omega \bar{\underline{\varepsilon}}^T \underline{\tau} d\Omega = \int_\Omega \bar{\underline{u}}^T \underline{f}^B d\Omega + \int_{S_f} \bar{\underline{u}}^{S_f T} \underline{f}^{S_f} dS \tag{14}$$

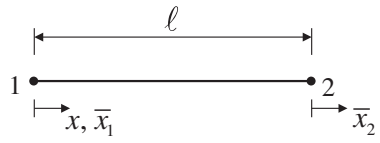

Fig. 3. One-dimensional (1D) element of length ℓ with the global and nodal local coordinate systems.

where, in the form of vectors, $\underline{u}(\underline{x})$ is the displacement, $\underline{\varepsilon}$ is the strain, $\underline{\tau}$ is the stress, $\underline{f}^B$ is the body force, $\underline{f}^{S_f}$ is the surface traction applied on S_f, and the overbar (–) denotes a virtual quantity.

The strain–displacement relation for element m is given by

$$\underline{\varepsilon}_h^{(m)} = \underline{B}^{(m)} \begin{bmatrix} \underline{u}^{(m)} \\ \underline{\tilde{a}}^{(m)} \end{bmatrix} = \underline{B}^{(m)} \underline{\tilde{u}}^{(m)} \tag{15}$$

with the obvious definition of $\underline{\tilde{u}}^{(m)}$. The stresses in element m are

$$\underline{\tau}_h^{(m)} = \underline{C}\underline{\varepsilon}_h^{(m)} = \underline{C}\underline{B}^{(m)}\underline{\tilde{u}}^{(m)} \tag{16}$$

where $\underline{C}$ is the stress–strain matrix.

Using these relations as usual for the element assemblage [1], we obtain

$$\underline{K}\underline{\tilde{u}} = \underline{R} \tag{17}$$

where $\underline{K}$ is the global stiffness matrix, $\underline{R} = \underline{R}_B + \underline{R}_S$ is the load vector, and $\underline{\tilde{u}}$ is the total solution vector listing all nodal displacements and cover coefficients. The stiffness matrix and load vectors are

$$\underline{K} = \sum_{m=1}^{e} \underline{K}^{(m)} = \sum_{m=1}^{e} \int_{\Omega^{(m)}} \underline{B}^{(m)T} \underline{C} \underline{B}^{(m)} d\Omega \tag{18}$$

$$\underline{R}_B = \sum_{m=1}^{e} \underline{R}_B^{(m)} = \sum_{m=1}^{e} \int_{\Omega^{(m)}} \begin{bmatrix} \underline{H}^{(m)} & \underline{\tilde{H}}^{(m)} \end{bmatrix}^T \underline{f}^B d\Omega \tag{19}$$

and

$$\underline{R}_S = \sum_{m=1}^{e} \underline{R}_S^{(m)} = \sum_{m=1}^{e} \int_{S_f^{(m)}} \begin{bmatrix} \underline{H}^{S_f^{(m)}} & \underline{\tilde{H}}^{S_f^{(m)}} \end{bmatrix}^T \underline{f}^{S_f} dS \tag{20}$$

where the summation signs imply the direct assemblage process [1].

2.4. Governing equations of heat transfer in solids

The principle of virtual temperatures for heat transfer in a solid is [1]

$$\int_\Omega k \nabla\bar{\theta} \cdot \nabla\theta d\Omega + \int_{S_c} \tilde{h}\bar{\theta}^S \theta^S dS = \int_{S_q} \bar{\theta}^S q^S dS + \int_{S_c} \tilde{h}\bar{\theta}^S \theta_e dS \tag{21}$$

where k is the thermal conductivity, $\tilde{h}$ is the heat transfer coefficient on S_c to the ambient temperature θ_e, and q^S is the heat flux applied onto S_q. Assuming a constant heat transfer coefficient $\tilde{h}$ and $\theta_e = 0$, we obtain

$$(\underline{K}^k + \underline{K}^c)\underline{\tilde{\theta}} = \underline{Q} \tag{22}$$

where $\underline{K}^k$ is the conductivity matrix

$$\underline{K}^k = \sum_{m=1}^{e} \int_{\Omega^{(m)}} \underline{B}^{(m)T} k^{(m)} \underline{B}^{(m)} d\Omega \tag{23}$$

with the temperature gradient matrix $\underline{B}^{(m)}$ given as

$$\underline{B}^{(m)} = \begin{bmatrix} \underline{H}_x^{(m)} & \underline{\tilde{H}}_x^{(m)} \\ \underline{H}_y^{(m)} & \underline{\tilde{H}}_y^{(m)} \end{bmatrix}. \tag{24}$$

Also, $\underline{K}^c$ is the convection matrix

$$\underline{K}^c = \tilde{h} \sum_{m=1}^{e} \int_{S_c^{(m)}} \begin{bmatrix} \underline{H}^{S(m)} & \underline{\tilde{H}}^{S(m)} \end{bmatrix}^T \begin{bmatrix} \underline{H}^{S(m)} & \underline{\tilde{H}}^{S(m)} \end{bmatrix} dS \tag{25}$$

with $S_c^{(m)}$ the element convection boundary. Finally, the heat input vector $\underline{Q}$ is given by

$$\underline{Q} = \sum_{m=1}^{e} \int_{S_q^{(m)}} \begin{bmatrix} \underline{H}^{S(m)} & \underline{\tilde{H}}^{S(m)} \end{bmatrix}^T q^S dS \tag{26}$$

in which q^S represents the applied heat flux input on the element boundary that is part of S_q.

3. Stability and convergence of the scheme

In this section we present a sufficient condition that guarantees a positive definite global system matrix and show results regarding the convergence of the scheme. We consider a linear elastic structural problem, but the conclusions are also directly applicable to solutions in other problem categories.

3.1. Stability of the scheme

In order to have well-posed discretized equations, the finite element matrix $\underline{K}$ in Eq. (17) should be positive definite once

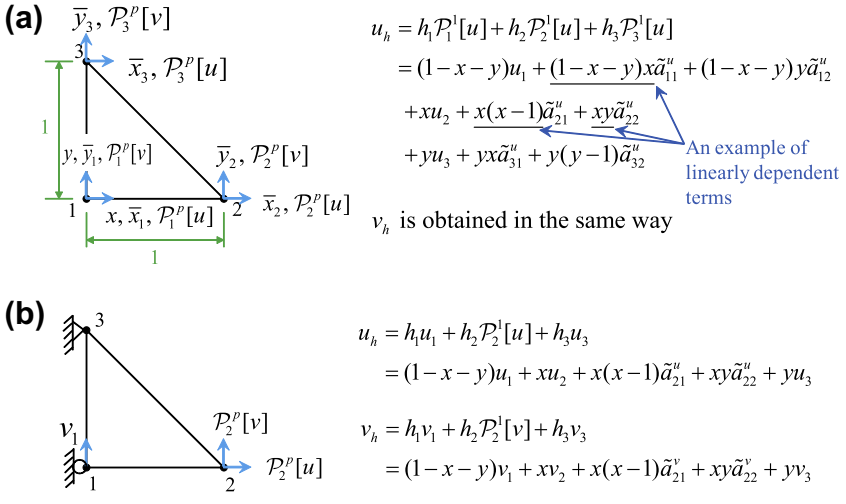

Fig. 4. Linear cover interpolation functions on a 3-node element: (a) linearly dependent interpolations with linear covers ($p = 1$), (b) linearly independent interpolations with prescribed boundary conditions ($p = 1$).

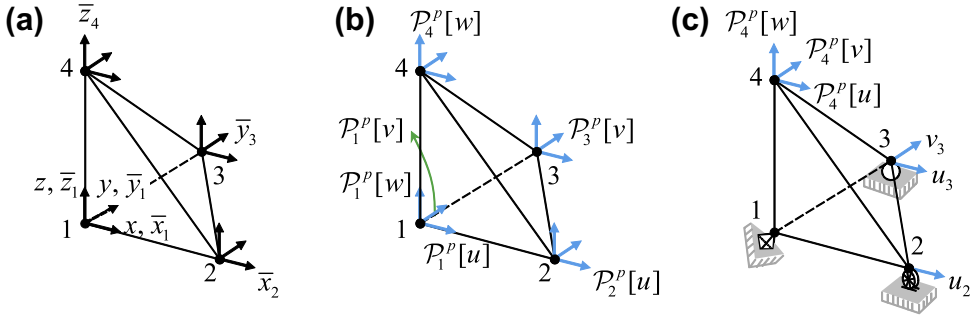

Fig. 5. Cover interpolation functions for a 4-node tetrahedral element: (a) global and nodal local coordinate systems, (b) all degrees of freedom, and (c) degrees of freedom after removing rigid body modes.

Fig. 6. One-dimensional bar model to investigate condition number, $L = 1, 10, 100$.

appropriate boundary conditions have been applied (to prevent rigid body motions).

In the following we consider the 1D, 2D and 3D analysis cases, using respectively the 2-node, 3-node and 4-node low-order elements, because we focus on improving the performance of discretizations using these elements.

Our goal is to show that the following property holds:

Property I. *If a mesh of traditional finite elements is properly restrained so that no rigid body modes are present (through prescribed u_i, v_i and w_i, as applicable, degrees of freedom) and if then covers are introduced but with no cover degrees of freedom $\underline{\tilde{a}}_i$ at the nodes with any prescribed degrees of freedom, then the resulting stiffness matrix $\underline{K}$ is positive definite.* □

To show that Property I holds, we first consider a single element, see Fig. 3. The interpolation functions for a 1D element with linear covers are

$$u_h = h_1 u_1 + h_1 \bar{x}_1 \tilde{a}_1 + h_2 u_2 + h_2 \bar{x}_2 \tilde{a}_2 \tag{27}$$

where

$$\bar{x}_1 = x, \quad \bar{x}_2 = x - \ell \tag{28}$$

so that Eq. (27) becomes

$$u_h = \left(1 - \frac{x}{\ell}\right) u_1 + \underline{\left(1 - \frac{x}{\ell}\right) x \tilde{a}_1} + \left(\frac{x}{\ell}\right) u_2 + \underline{\left(\frac{x}{\ell}\right)(x - \ell)\tilde{a}_2}. \tag{29}$$

Using quadratic covers we have

$$u_h = h_1 u_1 + h_1 \begin{bmatrix} \bar{x}_1 & \bar{x}_1^2 \end{bmatrix} \underline{\tilde{a}}_1 + h_2 u_2 + h_2 \begin{bmatrix} \bar{x}_2 & \bar{x}_2^2 \end{bmatrix} \underline{\tilde{a}}_2 \tag{30}$$

and in terms of x only we obtain

$$u_h = \left(1 - \frac{x}{\ell}\right) u_1 + \underline{\left(1 - \frac{x}{\ell}\right) x \tilde{a}_{11}} + \left(1 - \frac{x}{\ell}\right) x^2 \tilde{a}_{12} + \left(\frac{x}{\ell}\right) u_2 + \underline{\left(\frac{x}{\ell}\right)(x - \ell)\tilde{a}_{21}} + \left(\frac{x}{\ell}\right)(x - \ell)^2 \tilde{a}_{22}. \tag{31}$$

We can see that the functions in the interpolations are linearly dependent due to degrees of freedom in $\underline{\tilde{a}}_1$ and $\underline{\tilde{a}}_2$. In Eqs. (29) and (31) we have underlined the linearly dependent terms.

However, assume that we impose at node 1 the displacement u_1 (as usual, to take out the rigid body mode) and also eliminate the cover degrees of freedom $\underline{\tilde{a}}_1$ at that node. Then the remaining interpolation functions are linearly independent, for the linear cover

$$u_h = \left(1 - \frac{x}{\ell}\right) u_1 + \left(\frac{x}{\ell}\right) u_2 + \left(\frac{x}{\ell}\right)(x - \ell)\tilde{a}_2 \tag{32}$$

where u_1 would now be prescribed, and for the quadratic cover

$$u_h = \left(1 - \frac{x}{\ell}\right) u_1 + \left(\frac{x}{\ell}\right) u_2 + \left(\frac{x}{\ell}\right)(x - \ell)\tilde{a}_{21} + \left(\frac{x}{\ell}\right)(x - \ell)^2 \tilde{a}_{22} \tag{33}$$

where again u_1 would be prescribed. Figs. 4 and 5 give the corresponding interpolation functions for a 3-node triangular element and a 4-node tetrahedral element, respectively. Here too we see that the interpolation functions are linearly independent provided the procedure in Property I is used. In 2D, if the displacements are prescribed at nodes 1 and 3, as in Fig. 4, the cover degrees of freedom in $\underline{\tilde{a}}_1$ and $\underline{\tilde{a}}_3$ are all not applied, and we have the linearly independent interpolations

$$\begin{aligned} u_h &= (1 - x - y)u_1 + xu_2 + x(x-1)\tilde{a}_{21}^u + xy\tilde{a}_{22}^u + yu_3 \\ v_h &= (1 - x - y)v_1 + xv_2 + x(x-1)\tilde{a}_{21}^v + xy\tilde{a}_{22}^v + yv_3. \end{aligned} \tag{34}$$

In addition we also would have $u_1 = u_3 = v_3 = 0$. In 3D, we similarly have, with $p = 1$,

$$\begin{aligned} u_h &= (1-x-y-z)u_1 + xu_2 + yu_3 + zu_4 + zx\tilde{a}_{41}^u + zy\tilde{a}_{42}^u + z(z-1)\tilde{a}_{43}^u \\ v_h &= (1-x-y-z)v_1 + xv_2 + yv_3 + zv_4 + zx\tilde{a}_{41}^v + zy\tilde{a}_{42}^v + z(z-1)\tilde{a}_{43}^v \\ w_h &= (1-x-y-z)w_1 + xw_2 + yw_3 + zw_4 + zx\tilde{a}_{41}^w + zy\tilde{a}_{42}^w + z(z-1)\tilde{a}_{43}^w. \end{aligned} \tag{35}$$

Table 1
Condition numbers of the one-dimensional bar model.

Domain size	Number of elements	2	4	8	16	32	64	128
For all L	2-node elements	6.8e0	2.9e1	1.1e2	4.4e2	1.7e3	6.7e3	2.7e4
	3-node elements	3.8e1	1.5e2	5.8e2	2.3e3	9.0e3	3.6e4	1.4e5
$L = 1$	$\mathcal{IC}^1$	8.2e1	1.4e3	2.2e4	3.4e5	5.2e6	8.3e7	1.3e9
	$\mathcal{IC}^2$	2.8e3	1.8e5	1.1e7	6.9e8	4.3e10	2.7e12	1.7e14
$L = 10$	$\mathcal{IC}^1$	5.7e1	6.1e1	2.2e2	3.4e3	5.2e4	8.3e5	1.3e7
	$\mathcal{IC}^2$	4.6e2	1.4e3	2.2e4	1.3e6	7.7e7	4.8e9	3.0e11
$L = 100$	$\mathcal{IC}^1$	5.7e3	6.1e3	5.9e3	5.7e3	5.6e3	8.3e3	1.3e5
	$\mathcal{IC}^2$	4.5e6	1.0e6	4.3e5	1.6e6	5.9e6	4.6e7	2.9e9
For all L and cover DOFs normalized	$\mathcal{IC}^1$	2.1e1	8.8e1	3.4e2	1.3e3	5.1e3	2.0e4	8.0e4
	$\mathcal{IC}^2$	2.9e2	2.9e3	3.5e4	4.8e5	7.2e6	1.1e8	1.8e9

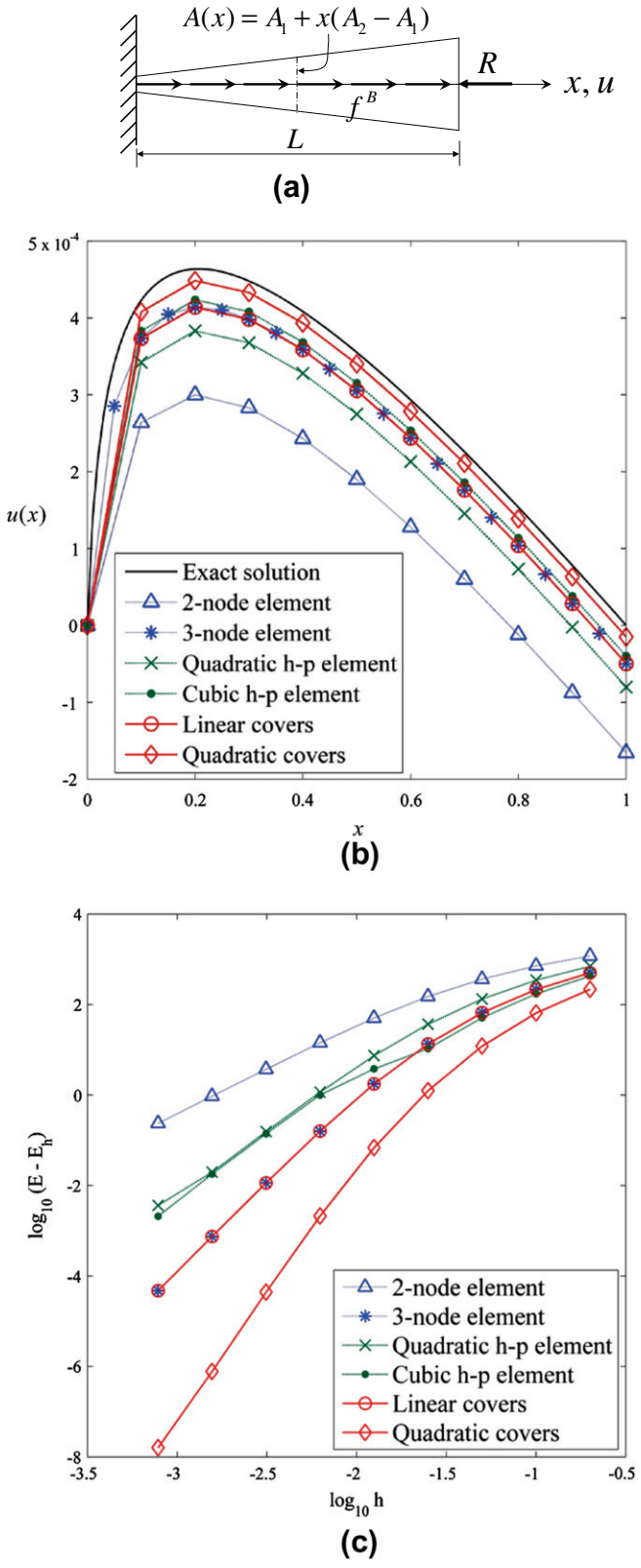

Fig. 7. Convergence study of 1D bar problem: (a) problem description, $E = 2.0 \times 10^{10}$, $A_1 = 0.01$, $A_2 = 1$, $L = 1$, $R = 1586 \times 10^4$, $f^B = 2 \times 10^7$, (b) displacements obtained with mesh of 10 elements, and (c) convergence curves of strain energy.

In addition, we would also have displacements prescribed to be zero at nodes 1, 2 and 3, as shown in Fig. 5.

Table 2
1D bar problem: summary of calculated orders of convergence of strain energy.

	2-node elements	3-node elements	$\mathcal{F}_D^{1,2}$	$\mathcal{F}_D^{1,3}$	$\mathcal{IC}^1$	$\mathcal{IC}^2$
Numerical results	1.97	3.91	2.79	2.97	3.91	5.69

This implies that $\underline{K}$ is positive definite for the single elements considered provided the rigid body modes have been removed, as usual by constraining appropriate degrees of freedom, with all $\tilde{\underline{a}}_i$ degrees of freedom also removed at the nodes with any prescribed displacements.

Consider now that additional elements are attached to these single elements, with no further $\underline{u}_i$ degrees of freedom prescribed and all $\tilde{\underline{a}}_i$ degrees of freedom free at the additional nodes used in the mesh. Then, by the above argument, for any nonzero values of the $\underline{u}_i$ and $\tilde{\underline{a}}_i$ degrees of freedom in the mesh, positive strain energy is stored in the mesh. Therefore, all eigenvalues of $\underline{K}$ are positive, which means that the matrix $\underline{K}$ in Eq. (17) is positive definite [1].

This result was already given in Ref. [54] based on numerical experiments, where it is also stated that, for example, using the 4-node quadrilateral 2D element the above approach may not be sufficient to obtain a positive definite matrix $\underline{K}$. Our reasoning given here can directly be used to show that this is indeed the case.

Of course, the condition number of the $\underline{K}$ matrix will increase as we refine the mesh. Fig. 6 shows a 1D case considered and Table 1 gives the condition numbers of $\underline{K}$ using the traditional 1D 2-node and 3-node elements, and the 2-node element with linear and quadratic covers, as the mesh is refined. The table shows that, without the normalization, the condition numbers using the $\mathcal{IC}^1$ scheme are acceptable but the condition numbers with the $\mathcal{IC}^2$ scheme are quite high. These condition numbers are considerably better when the normalization of the cover degrees of freedom by a characteristic length of the elements in the mesh is employed, like in Ref. [52], and here, of course, we naturally use $\hat{h} = h$ (the element size).

In practice, when solving 2D and 3D problems, many more degrees of freedom are usually constrained than only those to remove the rigid body modes, and the $\tilde{\underline{a}}_i$ degrees of freedom at all those nodes would then also be removed. Therefore, we focused in our discussion above on the worst case that may arise, and hence Property I always holds.

3.2. Convergence of the scheme

Since the coefficient matrix is positive definite, we can solve a sequence of meshes and estimate the solution errors measured by [1]

$$E - E_h \leqslant ch^{\alpha} \tag{36}$$

where, as usual, $E = \frac{1}{2}a(\underline{u}, \underline{u})$, with $a(\cdot,\cdot)$ being the bilinear form of the elasticity (or heat transfer, etc.) problem considered, h is the element size and α is the order of convergence. Using the equality sign, we obtain

$$\log(E - E_h) = \log c + \alpha \log h. \tag{37}$$

In practice we use the exact solution – or a very fine mesh of reliable finite elements to obtain a very close approximation thereof, called the reference solution – to evaluate E. We use Eq. (37) to estimate the order of convergence in the following example solutions. Furthermore, the relative error is given by $(E - E_h)/E$.

3.2.1. 1D bar analysis

Consider the one-dimensional bar shown in Fig. 7(a). The exact response solution is easily obtained and also given in Ref. [55].

Since we want to compare our cover solution results with those obtained using the proposed schemes in Refs. [51,52], we use the notation employed in Ref. [50]. Therefore $\mathcal{F}_{\mathcal{D}}^{m,p}$ denotes the h-p cloud function space constructed with traditional element interpolations of degree m that are enriched with monomials of degree $m+1$ to $m+p-1$. We shall use $m=1$ in the example below, and we note that our $\mathcal{IC}^p$ schemes use a complete set of polynomial bases of degree p. Using successive uniform mesh refinements with elements of equal length, six schemes are evaluated. The schemes used in the mesh are

- the traditional linear 2-node element $\mathcal{F}_{\mathcal{D}}^{1,0} = \mathcal{IC}^0$
- the traditional quadratic 3-node element $\mathcal{F}_{\mathcal{D}}^{2,0}$
- the quadratic h-p element $\mathcal{F}_{\mathcal{D}}^{1,2}$: {element basis functions} $\times\{1 \quad x^2\}$
- the cubic h-p element $\mathcal{F}_{\mathcal{D}}^{1,3}$: {element basis functions} $\times\{1 \quad x^2 \quad x^3\}$
- the 2-node elements with linear covers $\mathcal{IC}^1$: {element basis functions} $\times\{1 \quad \bar{x}_i\}, \ \forall i$
- the 2-node elements with quadratic covers $\mathcal{IC}^2$: {element basis functions} $\times\{1 \quad \bar{x}_i \quad \bar{x}_i^2\}, \ \forall i$

For all simulations, no polynomial cover term is introduced at the boundaries where the essential boundary conditions are imposed. Note that the x basis is missing in the $\mathcal{F}_{\mathcal{D}}^{m,p}$ schemes and that with these schemes the global coordinates are used, whereas in the $\mathcal{IC}^p$ schemes local coordinate systems are employed.

Fig. 7(b) shows the displacement fields calculated using meshes of 10 elements, and Fig. 7(c) shows the convergence in the energy norm when systematically refined meshes are used. Among all schemes implemented, using quadratic interpolation covers provides the best accuracy in both displacements and strain energies. One interesting but expected fact is that there is little difference between the solutions using linear covers on the 2-node elements

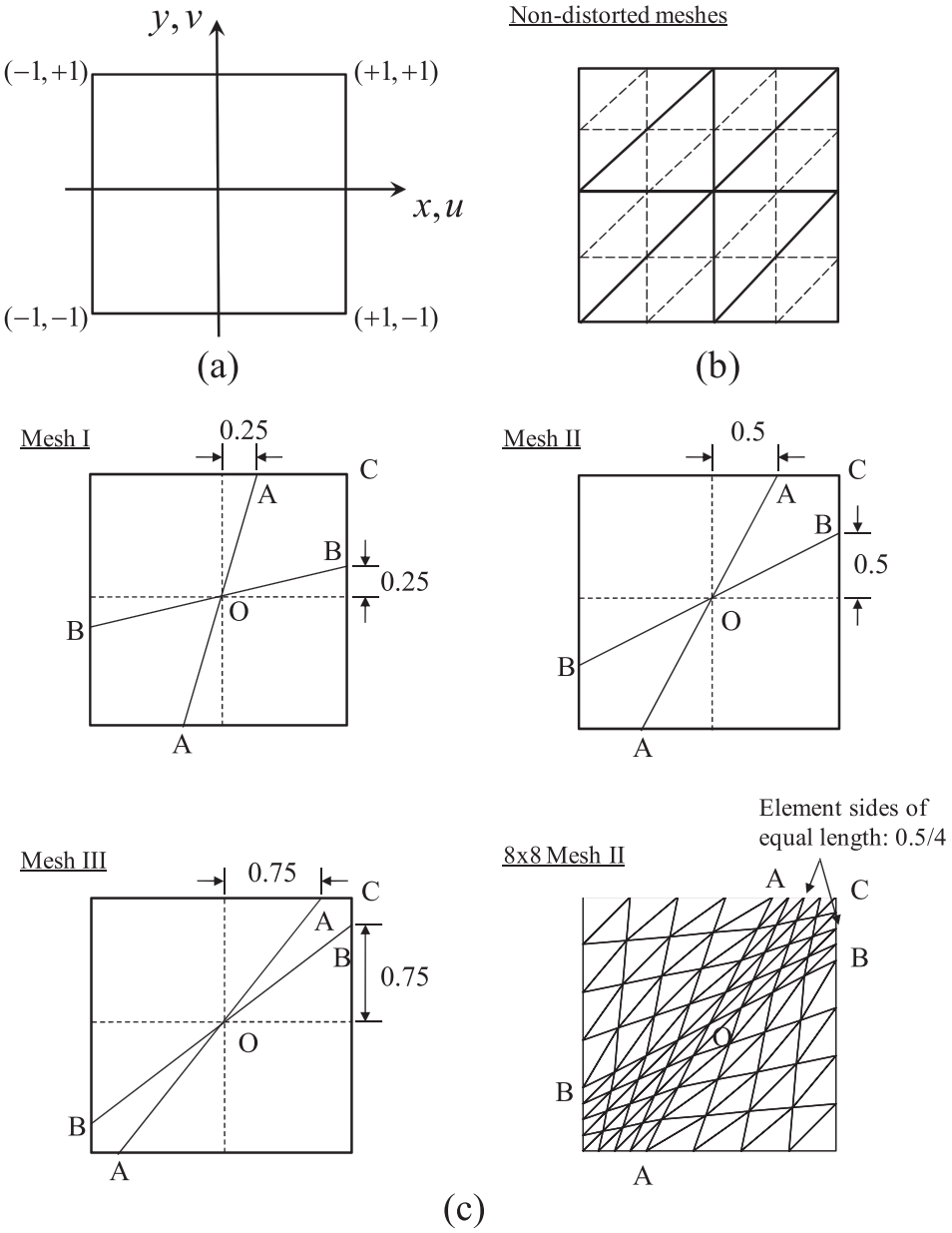

Fig. 8. Ad-hoc test problem: (a) problem domain, $E = 7.2 \times 10^6$, $\nu = 0.3$, (b) typical non-distorted meshes, (c) induced distortions.

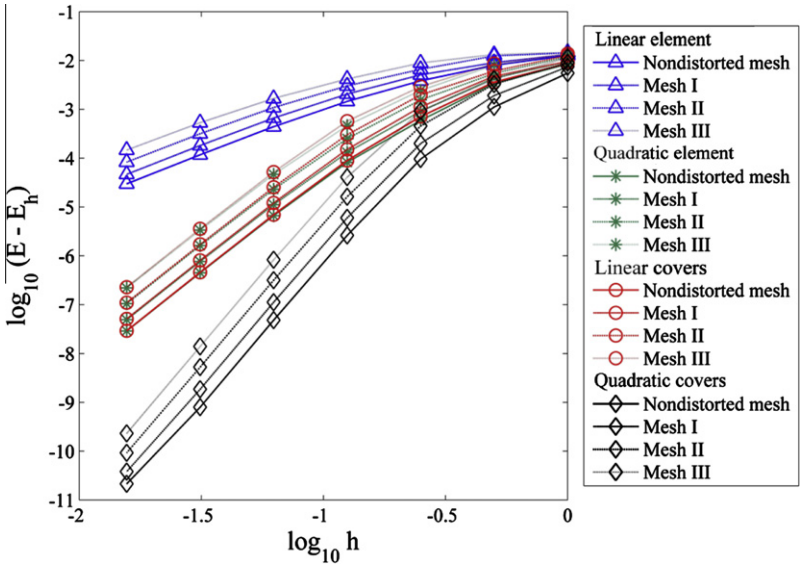

Fig. 9. Ad-hoc test problem: convergence curves for strain energy.

Table 3
Ad-hoc problem: summary of calculated orders of convergence of strain energy.

	Non-distorted Mesh	Distorted Meshes		
		Mesh I	Mesh II	Mesh III
Linear 3-node elements	1.95	1.92	1.86	1.76
Quadratic 6-node elements	3.93	3.91	3.89	3.86
Linear covers $\mathcal{IC}^1$	3.95	3.94	3.93	3.92
Quadratic covers $\mathcal{IC}^2$	5.84	5.83	5.80	5.76

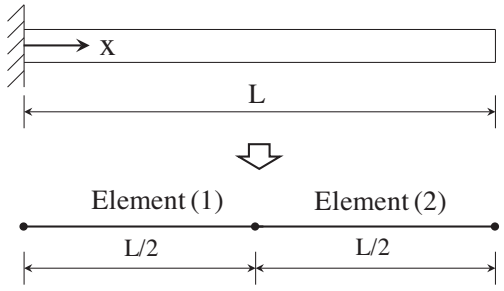

Fig. 10. Model of two elements to evaluate matrix conditioning, $E = 1.0,\ A = 1$.

(the $\mathcal{IC}^1$ scheme) and the solutions using the standard 3-node quadratic finite element.

We summarize in Table 2 the numerically calculated convergence orders of each scheme. The standard and our enriched finite element methods reproduce the expected values, while the $\mathcal{F}_{\mathcal{D}}^{m,p}$ schemes do not perform well, see also Fig. 7(c). We also observed that the coefficient matrices using the $\mathcal{F}_{\mathcal{D}}^{m,p}$ scheme of Ref. [51] become quite rapidly ill-conditioned as the mesh is refined, which is partly due to the terms used in the displacement interpolations and partly due to the use of global coordinates, see Section 4.1.

3.2.2. Ad hoc in-plane analysis

In Section 3.2.1, we have seen that the choice of a complete set of polynomial bases provides stable and accurate results in a 1D analysis. Here we investigate the convergence behavior and the sensitivity to mesh distortions in a 2D analysis.

Consider the ad hoc plane stress test problem shown in Fig. 8(a), see Ref. [1]. For the given in-plane displacements

Table 4
1D two-element problem: comparison of condition numbers using global and local coordinate systems.

Scheme used	Length	$\mathcal{IC}^1$	$\mathcal{IC}^2$	$\mathcal{F}_{\mathcal{D}}^{1,2}$	$\mathcal{F}_{\mathcal{D}}^{1,3}$
Global coordinate system without normalization	$L = 1$	2.3e2	1.3e4	1.7e2	3.2e4
	$L = 10$	4.3e3	3.5e6	2.5e5	8.6e7
	$L = 100$	4.2e5	3.2e10	2.5e9	8.5e13
Local coordinate system without normalization	$L = 1$	8.2e1	2.8e3	3.3e2	2.7e4
	$L = 10$	5.7e1	4.6e2	4.5e2	7.1e3
	$L = 100$	5.7e3	4.5e6	4.5e6	7.1e9
Local coordinate system with normalization	For all L	2.1e1	2.9e2	2.1e1	6.0e2

$$u = (1-x^2)^2(1-y^2)^2 e^{ky}\cos kx$$
$$v = (1-x^2)^2(1-y^2)^2 e^{ky}\sin kx \tag{38}$$

we can establish the corresponding body forces

$$f_x^B = -\left(\frac{\partial \tau_{xx}}{\partial x} + \frac{\partial \tau_{xy}}{\partial y}\right), \quad f_y^B = -\left(\frac{\partial \tau_{yy}}{\partial y} + \frac{\partial \tau_{yx}}{\partial x}\right) \tag{39}$$

to satisfy equilibrium. Then Eq. (38) gives the exact solution to the problem. We use these body forces to construct the load vector, and compare the numerical results of E_h with the analytical value E (see Eq. (37)) obtained using Eq. (38). For the solution, we use $k = 5$ and the displacement boundary conditions are applied along the line $y = -1$, where all cover degrees of freedom are removed.

Fig. 8(b) shows the first two meshes used, in undistorted form. The meshes are constructed by starting with triangular elements of diagonal length $\sqrt{2}$, then subdividing each element into four equal triangular elements to obtain the second mesh (see dashed lines) where the element size is exactly half of the first one, and continuing the process. Fig. 8(c) gives the systematic element distortion process used. We consider three different degrees of distortion categorized by Meshes I, II and III in the figure. The lines A–A and B–B are drawn, and the sides AC, BC, OB, OA are subdivided into equal lengths to form the elements in the domain ACBO. We proceed similarly for the other domains.

Since the $\mathcal{F}_{\mathcal{D}}^{m,p}(p \geqslant 1)$ discretizations studied in Section 3.2.1 are not robust, we only give comparisons of the performance of the standard finite elements and our cover schemes enriching the linear element. The convergence behaviors are summarized

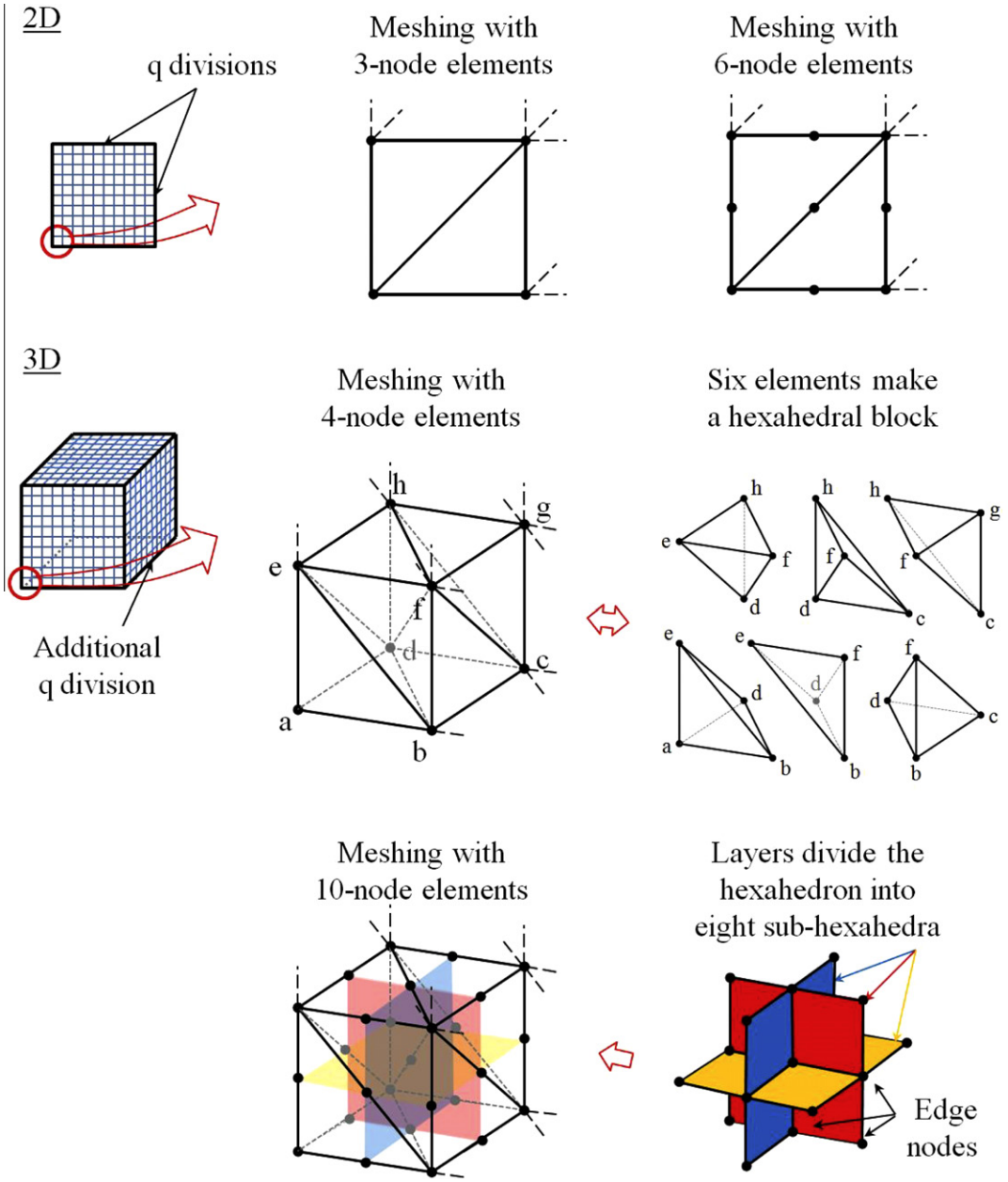

Fig. 11. Meshes for ad hoc test problem; 3-node triangular and 4-node tetrahedral elements are used.

in Fig. 9 and Table 3. When non-distorted meshes are used, the calculated orders compare well with the theoretical estimates. As seen in Fig. 9, using the quadratic covers $\mathcal{IC}^2$ gives the highest convergence rate, and the linear cover scheme $\mathcal{IC}^1$ and quadratic finite elements $\mathcal{F}_{\mathcal{D}}^{2,0}$ perform almost equally. As the degree of distortion increases from Mesh I to Mesh III, the convergence curves shift upwards in all schemes. However, if the loss in solution accuracy is deemed significant, a higher order cover interpolation can be used to obtain more accurate results. This approach can be valuable since different covers can be employed in different regions of the mesh.

4. Numerical aspects

Two numerical aspects of importance are the conditioning of the stiffness matrix of the complete finite element system and the expense of using the solution procedure.

4.1. Matrix conditioning

As mentioned already, the use of local nodal coordinates is important. Consider the simple one-dimensional 2-element model shown in Fig. 10; we shall study the cases $L = 1, 10, 100$.

Table 4 gives the condition numbers of the stiffness matrices for the schemes introduced in Section 3.2.1 when global and local coordinates are used. As shown in the table, when the global coordinate is used, the condition numbers are not only more sensitive to the domain size but are also in general larger. Hence the solution robustness is increased by using local coordinates for, both, the $\mathcal{F}_{\mathcal{D}}^{m,p}$ and $\mathcal{IC}^p$ schemes. However, the table also shows that the conditioning of the coefficient matrix is even further increased by using the normalization of the cover degrees of freedom by an element characteristic length as mentioned in Section 2.1, and proposed in Ref. [52]. In this example we naturally use $\hat{h} = h$.

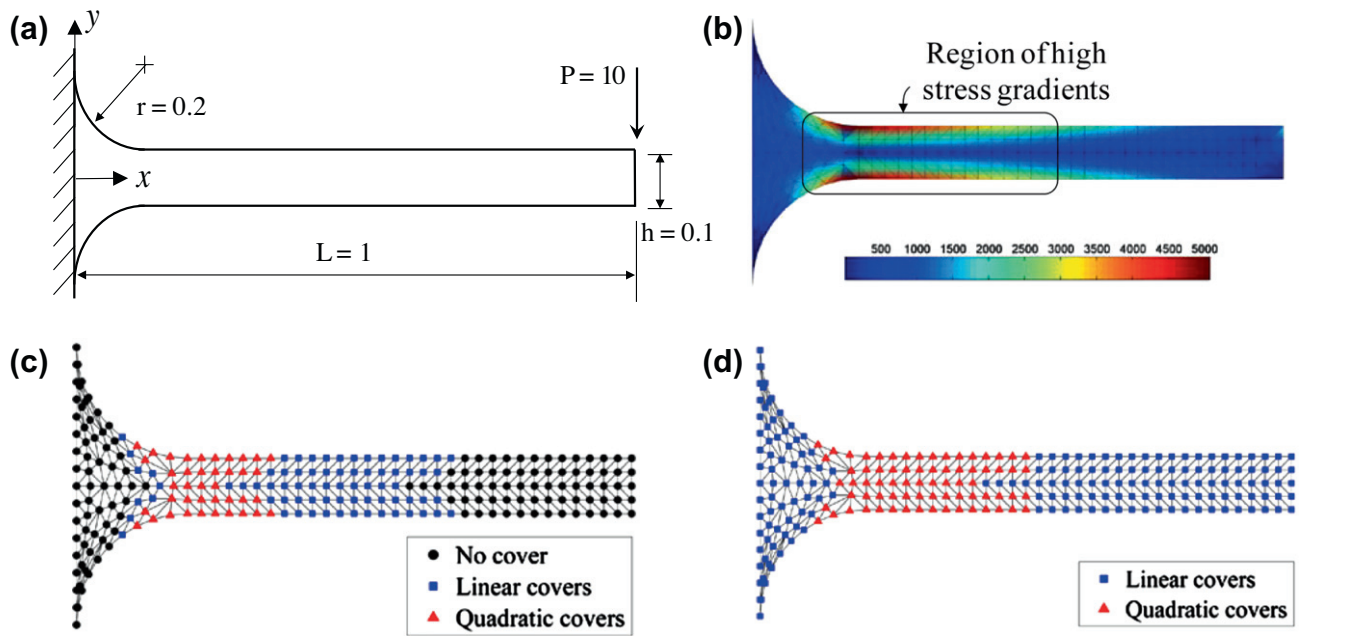

Fig. 12. Analysis of cantilever beam with large fillet radius: (a) problem description, $E = 7.2 \times 10^9$, $\nu = 0.3$, (b) von Mises stress field obtained with 392 elements and linear covers, (c) mixed scheme $\mathcal{IC}^{\{0,1,2\}}$ is used, (d) mixed scheme $\mathcal{IC}^{\{1,2\}}$ is used (the covers at the fixed boundary are not used in the solution).

4.2. Numerical expense

It is of value to compare the numerical operations required when using the cover interpolations versus using higher-order traditional finite elements. In both cases, of course, symmetric stiffness or coefficient matrices are generated. To obtain some insight into the computational efforts needed in the respective solutions, we focus on the solution of the governing equations obtained using direct Gauss elimination, in which the factorization of the stiffness matrices represents the major expense.

The numerical operations for the factorizations of the *banded* stiffness matrices are then approximately $(1/2)nm_K^2$ where n is the number of equations and m_K is the (effective) half-bandwidth [1]. For an evaluation, consider the solution of the problem in Fig. 8 using the $\mathcal{IC}^1$ scheme and the use of 6-node triangular elements, with the same meshes. As we have seen, about the same solution accuracy is obtained using these two discretizations in this 2D problem (but this may not hold in the solution of a true 3D problem).

Let the number of elements along the sides be q, and let us ignore in all cases the zero entries within the band, then we have for this 2D problem, see Fig. 11,

- for the $\mathcal{IC}^1$ solution, $n \simeq q \times q \times 2 \times 3$, $m_K \simeq q \times 2 \times 3$;
- for the solution using the 6-node element, $n \simeq 2q \times 2q \times 2$, $m_K \simeq 2q \times 2 \times 2$.

The ratio of numerical operations referred to above is 27/64, and while this ratio pertains to a very specific problem solution and is approximate, solutions with covers in general can be expected to be reasonably effective.

Table 5
Analysis of cantilever beam: comparison of total numbers of degrees of freedom (DOFs) and errors in calculated strain energies.

	Reference	Linear elements	$\mathcal{IC}^1$	$\mathcal{IC}^2$	$\mathcal{IC}^{\{0,1,2\}}$	$\mathcal{IC}^{\{1,2\}}$
DOFs	20,342	498	1494	2988	1194	1932
$E_{ref} - E_h$	0	7.01e−7	2.92e−8	2.54e−8	1.13e−7	2.82e−8
Percentage (%)	0	17.7	0.7	0.6	2.9	0.7

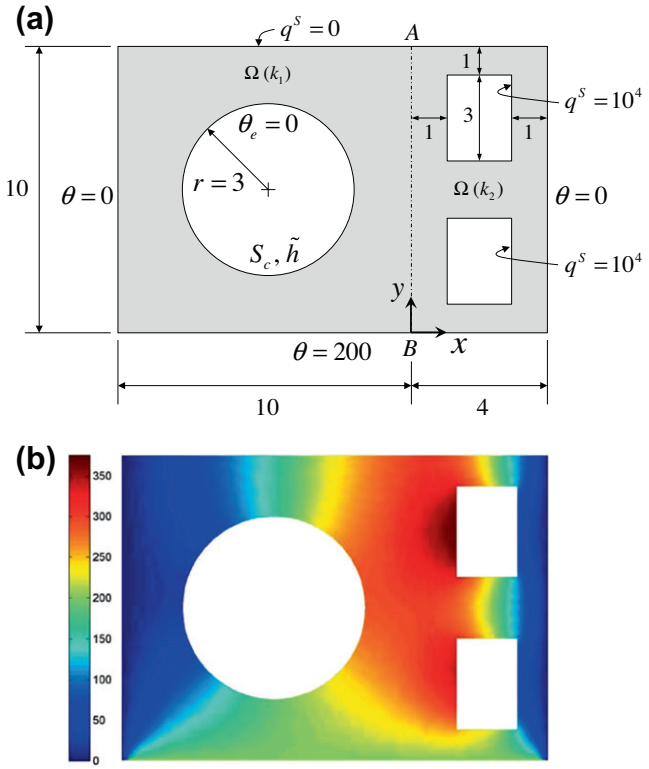

Fig. 13. Two-dimensional heat transfer problem: (a) problem description, $k_1 = 50$, $k_2 = 100$, $\tilde{h} = 1$, (b) calculated temperature distribution.

In a three-dimensional analysis of this problem, we also consider q divisions into the third direction, see Fig. 11 (where we use 6 tetrahedral elements per hexahedral domain). Comparing the use of 4-node tetrahedral elements with linear covers and the use of the same mesh with 10-node tetrahedral elements, we have

- for the $\mathcal{IC}^1$ solution, $n \simeq q \times q \times q \times 3 \times 4$, $m_K \simeq q \times q \times 3 \times 4$;
- for the solution using the 10-node element, $n \simeq 2q \times 2q \times 2q \times 3$, $m_K \simeq 2q \times 2q \times 2 \times 3$.

The ratio is now 1/8 and hence here, for this problem solution, an even smaller effort is needed when using covers.

But in particular, a major benefit of using the cover interpolations is that covers need not be used throughout the complete analysis domain but can be added in a mixed manner in those regions where they provide good benefit for solution accuracy, as we shall demonstrate next in the example solutions.

5. Illustrative example solutions

In this section, we present some two and three-dimensional simulation results to compare the performance of the standard

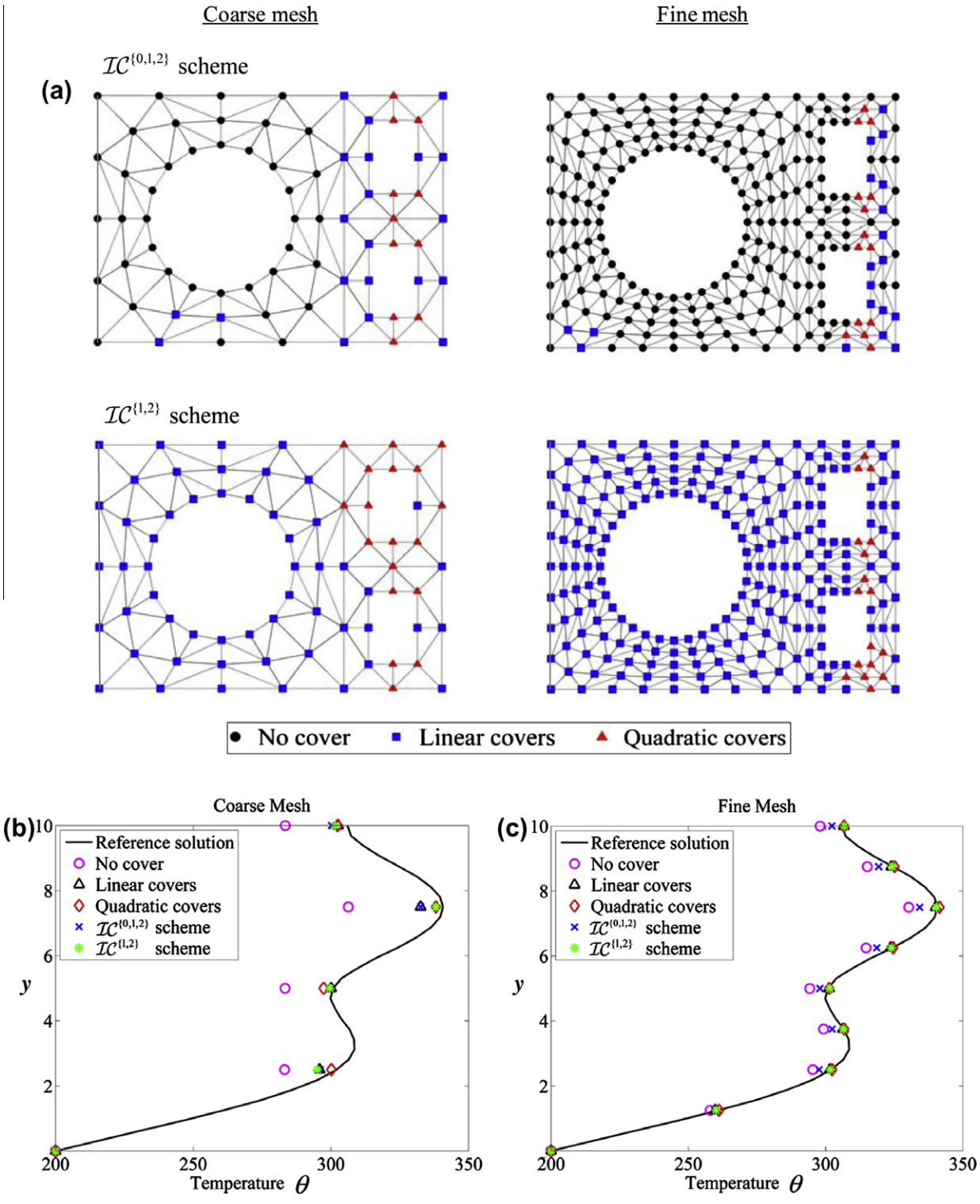

Fig. 14. Heat transfer analysis using standard and enriched schemes: (a) adaptive interpolations used for coarse and fine meshes (the covers at the boundaries with prescribed temperatures are not used in the solution), (b) and (c) temperature plots along the evaluation line $(0, y)$.

Table 6
Analysis of heat transfer problem: comparison of total number of degrees of freedom (DOFs) and relative errors.

		Linear elements	$\mathcal{IC}^1$	$\mathcal{IC}^2$	$\mathcal{IC}^{\{0,1,2\}}$	$\mathcal{IC}^{\{1,2\}}$
Coarse mesh	DOFs	72	216	432	135	237
	Errors (%)	8.90	3.19	2.41	3.44	2.86
Fine mesh	DOFs	242	726	1452	295	750
	Errors (%)	2.71	0.48	0.27	1.75	0.45

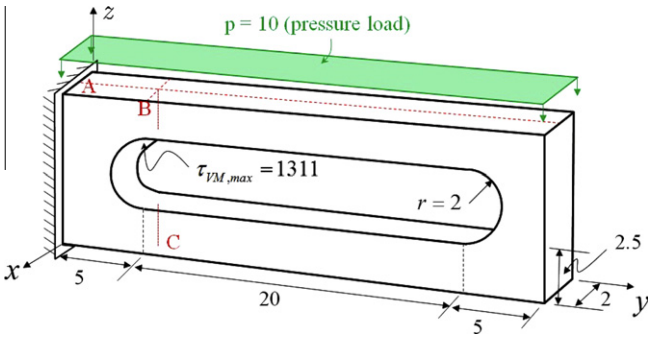

Fig. 15. Three-dimensional machine tool jig, material properties $E = 7.2 \times 10^{10}$ and $\nu = 0.3$.

and enriched finite elements, and also to illustrate the use of different orders of covers over the solution domains. The computed results are identical whether the mentioned normalization of the cover degrees of freedom is used or not.

In order to determine a proper mixed cover series $\{ad\}$, see Eq. (13), and the regions where covers might be used, we establish a first numerical solution, with or without covers (depending on the simulation purpose). We evaluate the element stress or temperature gradients and then establish whether covers, and of which order and in which regions, should be applied. Of course, there are different ways to proceed in the choice of covers, and in the example solutions below we simply illustrate how different covers can be used and what effects these have on the solution accuracy.

5.1. Cantilever beam with fillets

Consider the two-dimensional cantilever beam in plane stress conditions subjected to a tip load shown in Fig. 12(a). An example von Mises stress plot obtained using the $\mathcal{IC}^1$ scheme is given in Fig. 12(b), where the high stress gradients in the fillets can be seen. For an effective analysis, different covers might be applied over the solution domain. Figs. 12(c) and (d) show two possible applications of covers. Fig. 12(c) refers to a scheme $\mathcal{IC}^{\{0,1,2\}}$ that applies constant, linear and quadratic covers and Fig. 12(d) refers to a scheme $\mathcal{IC}^{\{1,2\}}$, with which we expect a more accurate solution.

Since there is no exact solution to the problem, we measure the error on the reference solution obtained with a fine mesh of 2460 9-node quadrilateral elements. For the evaluations of the various schemes we always use a rather coarse mesh of 392 elements. Table 5 gives the relative errors in strain energies and the total number of degrees of freedom used.

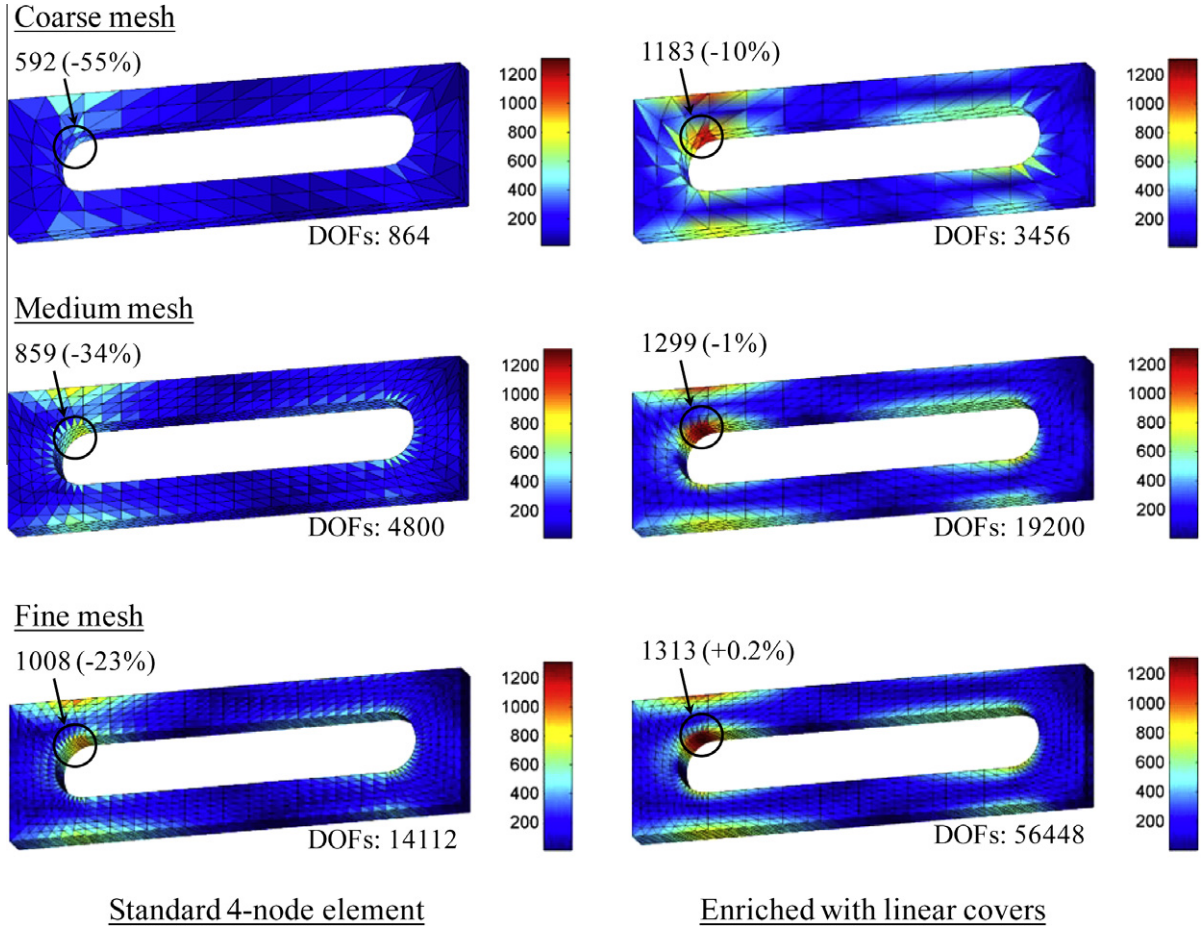

Fig. 16. von Mises stress results for the machine tool jig problem (DOFs = total number of degrees of freedom used).

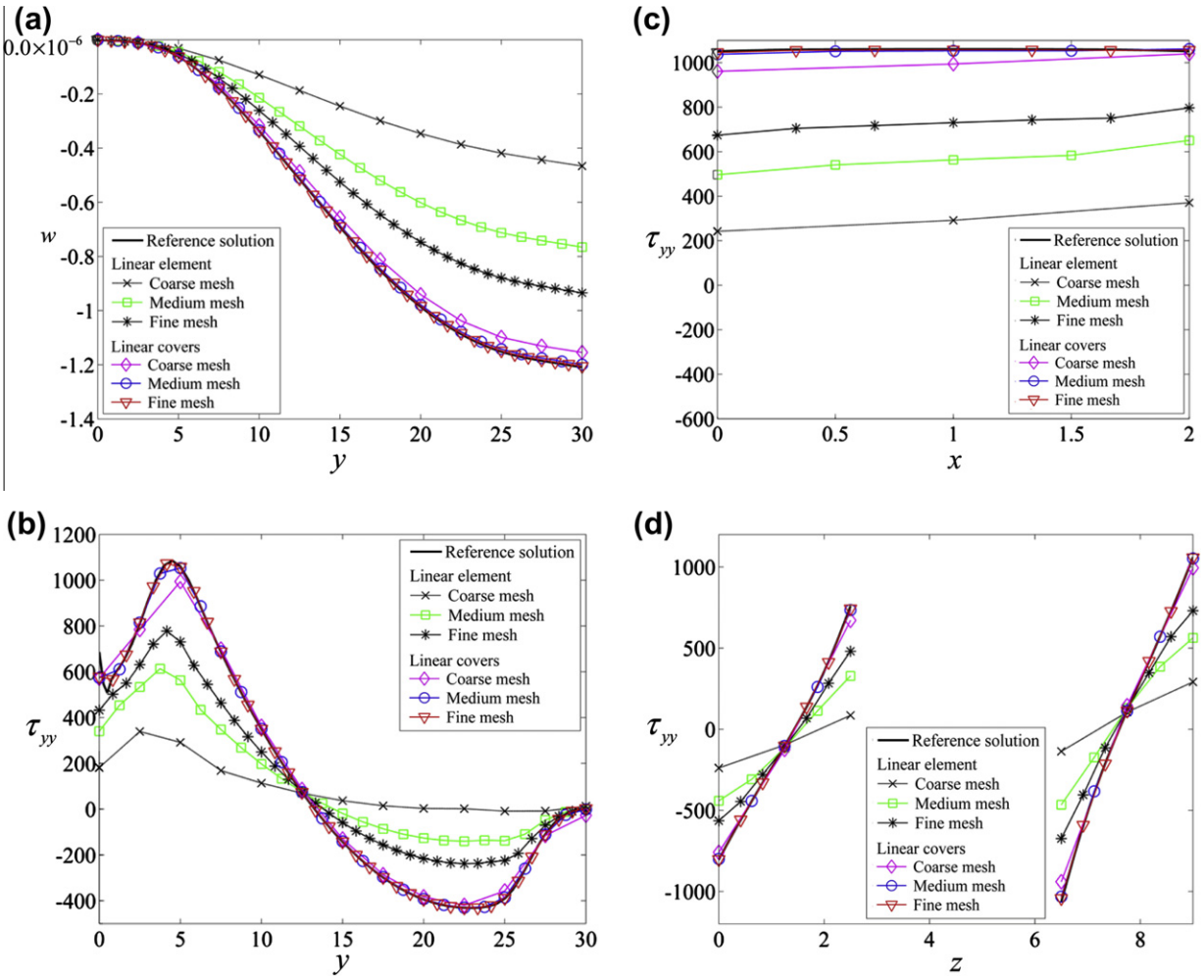

Fig. 17. Analysis of 3D tool jig, comparisons of results along the evaluation lines: (a) z-displacement along the line A, and (b)–(d) longitudinal normal stresses along the lines A, B and C, respectively.

As expected, the accuracy increases as the order of the interpolation covers increases, and the errors obtained using the interpolations $\mathcal{IC}^{\{0,1,2\}}$ and $\mathcal{IC}^{\{1,2\}}$ are in-between the errors measured using the traditional 3-node element and the $\mathcal{IC}^2$ interpolation. In particular, using the $\mathcal{IC}^1$ and $\mathcal{IC}^{\{1,2\}}$ schemes results in excellent accuracy compared to using the $\mathcal{IC}^2$ interpolation with a smaller number of degrees of freedom. These results illustrate that a proper choice of cover interpolations can be important.

5.2. Two-dimensional heat transfer

Fig. 13(a) shows the heat transfer problem solved. We obtained the reference solution using a very fine mesh of 12,288 9-node elements and show this solution in Fig. 13(b). For the evaluation of the various discretizations we use the calculated temperature along the line AB ($x = 0$ in Fig. 13(a)).

Fig. 14(a) shows two types of interpolations used with coarse and fine meshes. Again we use $\mathcal{IC}^{\{0,1,2\}}$ and $\mathcal{IC}^{\{1,2\}}$ schemes, in which the higher order covers are applied where temperature gradients are steep. As seen in Fig. 14(b), the enriched scheme solutions can provide good accuracy even using the coarse mesh. Note that the $\mathcal{IC}^{\{0,1,2\}}$ scheme solution given in Fig. 14(c) with the fine mesh is not accurate enough because a small number of interpolation covers are used.

Table 6 shows the relative errors obtained in the analyses using the standard, fully enriched and mixed schemes. We see that the use of the interpolation covers results into excellent overall accuracy, even with the coarse mesh, and the use of different covers in different parts of the problem domain can be beneficial.

5.3. Three-dimensional machine tool jig

Finally, we present a 3D analysis example, like considered in Refs. [55,56], see Fig. 15. The geometry of the machine tool jig is taken from Ref. [56]. The enriched interpolations for the 4-node tetrahedral elements used in the 3D solutions can directly be developed from the 2D interpolations derived in Section 2. Since, as discussed in Section 4.2, the $\mathcal{IC}^1$ scheme is more efficient than the use of quadratic finite elements, we only adopt the linear covers in this simulation and compare the results with the traditional 4-node element solutions.

We consider the structure subjected to a constant pressure load on its top surface, see Fig. 15. The maximum von Mises stress occurs at the round inner surface as marked in the figure. The error is measured with respect to the solution obtained with a very fine mesh of 16,000 27-node brick elements, leading to 423,360 degrees of freedom. To compare the displacement and stress results, we use the solutions along the dashed evaluation lines A, B, and C.

As seen in Figs. 16 and 17, the solution accuracy is significantly improved with the cover scheme. Using the enrichment scheme provides good agreement with the reference value of maximum von Mises stress, while the standard linear finite element solution

gives a 23-percent error in the von Mises stress with the finest mesh. We also give the total number of degrees of freedom used in the solutions in Fig. 16. Note that the use of the covers increases by 4 times the number of degrees of freedom that are employed (see Sections 2.2 and 4.2). It is interesting that the standard finite element fine mesh solution provides a significantly worse maximum von Mises stress prediction than the use of linear covers in the coarse mesh with only about one quarter of the number of degrees of freedom.

Fig. 17 shows the calculated z-displacement and longitudinal normal stress τ_{yy} (averaged at the nodes) along the evaluation lines. These plots confirm once more that the $\mathcal{IC}^1$ solution using the coarse mesh is more accurate than the standard finite element solution using the fine mesh. We also see that the $\mathcal{IC}^1$ solution using the medium mesh gives good displacement and stress predictions.

6. Concluding remarks

In this paper we focused on a general procedure to improve the displacement and stress predictions obtained using classical finite element methods by applying interpolation covers. As pointed out, the proposed scheme can be derived by various approaches and, in fact, the theory was presented earlier. Hence our objective in this paper was to investigate the effective use of the procedure for the low-order triangular 2D and tetrahedral 3D elements.

Covers as used in the numerical manifold method lead to a direct enrichment of the traditional finite element method. The cover scheme provides smoother solutions and higher order convergence, and can be used efficiently with relatively coarse meshes. An important aspect is that the interpolation space is enriched by the cover functions without changing the mesh topology. Reasonably coarse meshes might be used, and if the results obtained with the traditional finite elements are not acceptable, covers are applied to obtain improved solution results; hence, the adaptivity inherent in the approach has considerable potential.

The scheme we focused on employs local coordinate systems for the interpolation covers, possible normalization, and the cover terms are removed at boundaries with Dirichlet boundary conditions. This approach yields a nonsingular global stiffness matrix and reasonable matrix conditioning.

The estimation of the numerical expense indicates that using the cover scheme can be efficient. Also, the adaptive choice of cover functions provides good potential to minimize the need of mesh refinements. We illustrated the use of mixed cover schemes based on some gradients of the calculated solutions but of course other criteria can be employed. The cover functions can also be used to increase the solution accuracy when elements are quite distorted.

We should note that the cover scheme improves the displacement *and* stress predictions, as shown in the paper when using the 3-node triangular and 4-node tetrahedral elements, and not only the stress predictions as does, for example, the scheme of Payen–Bathe given in Ref. [57]. Of course, the added cost of solution using the cover scheme is quite significant whereas the cost to improve only the stresses is very small [57].

Considering future research, we only considered in this paper the linear time-independent analysis of solids and heat transfer. It would be valuable to develop the enrichment scheme for the solution of dynamic and general nonlinear problems, using the low-order solid elements, and for the analysis of shell structures using mixed interpolations [1,58,59]. Finally, the scheme should be tested thoroughly in all cases, in particular in 3D solutions, with respect to the accuracy obtained and the computational effort required, and would ideally be developed for use in a fully automatic adaptive procedure for linear and nonlinear analyses and the calculation of error measures.

References

[1] Bathe KJ. Finite Element Procedures. Cambridge, MA: Klaus-Jürgen Bathe; 2006.
[2] Kato K, Lee NS, Bathe KJ. Adaptive finite element analysis of large strain elastic response. Comput Struct 1993;47:829–55.
[3] Lee NS, Bathe KJ. Error indicators and adaptive remeshing in large deformation finite element analysis. Finite Elem Anal Des 1994;16:99–139.
[4] Zhu J, Gotoh M, Shang J, Sun ZG. An integrated FEM system facilitated with automatic remeshing. Met Mater 1998;4:657–61.
[5] Zhan M, Yuli L, He Y. Research on a new remeshing method for the 3D FEM simulation of blade forging. J Mater Process Technol 1999;94:231–4.
[6] Bathe KJ, Zhang H. A mesh adaptivity procedure for CFD & fluid-structure interactions. Comput Struct 2009;87:604–17.
[7] Bathe KJ, Almeida C. A simple and effective pipe elbow element – linear analysis. ASME J Appl Mech 1980;47:93–100.
[8] Bathe KJ, Almeida C, Ho LW. A simple and effective pipe elbow element – some nonlinear capabilities. Comput Struct 1983;17:659–67.
[9] Bathe KJ, Chaudhary A. On the displacement formulation of torsion of shafts with rectangular cross-sections. Int J Numer Methods Eng 1982;18:1565–8.
[10] Moes N, Dolbow J, Belytschko T. A finite element method for crack growth without remeshing. Int J Numer Methods Eng 1999;46:131–50.
[11] Belytschko T, Black T. Elastic crack growth in finite elements with minimal remeshing. Int J Numer Methods Eng 1999;45:601–20.
[12] Daux C, Moes N, Dolbow J, Sukumar N, Belytschko T. Arbitrary branched and intersecting cracks with the extended finite element method. Int J Numer Methods Eng 2000;48:1741–60.
[13] Abdelaziz Y, Hamouine A. A survey of the extended finite element. Comput Struct 2008;86:1141–51.
[14] Melenk JM, Babuška I. The partition of unity finite element method: basic theory and applications. Comput Methods Appl Mech Eng 1996;139:289–314.
[15] Babuška I, Melenk JM. The partition of unity method. Int J Numer Methods Eng 1997;40:727–58.
[16] Strouboulis T, Copps K, Babuška I. The generalized finite element method: an example of its implementation and illustration of its performance. Int J Numer Methods Eng 2000;47:1401–17.
[17] Strouboulis T, Copps K, Babuška I. The generalized finite element method. Comput Methods Appl Mech Eng 2001;190:4081–193.
[18] Belytschko T, Lu YY, Gu L. Element-free Galerkin methods. Int J Numer Methods Eng 1994;37:229–56.
[19] Liu WK, Jun S, Li S, Adee J, Belytschko T. Reproducing kernel particle methods for structural dynamics. Int J Numer Methods Eng 1995;38:1655–79.
[20] Duarte CA, Oden JT. H-p clouds – an h-p meshless method. Numer Methods Part D E 1996;12:673–705.
[21] Liszka TJ, Duarte CA, Tworzydlo WW. Hp-meshless cloud method. Comput Methods Appl Mech Eng 1996;139:263–88.
[22] Atluri SN, Zhu T. A new meshless local Petrov–Galerkin (MLPG) approach in computational mechanics. Comput Mech 1998;22:117–27.
[23] De S, Bathe KJ. The method of finite spheres. Comput Mech 2000;25:329–45.
[24] De S, Bathe KJ. Displacement/pressure mixed interpolation in the method of finite spheres. Int J Numer Methods Eng 2001;51:275–92.
[25] De S, Bathe KJ. Towards an efficient meshless computational technique: the method of finite spheres. Eng Comput 2001;18:170–92.
[26] Hong JW, Bathe KJ. Coupling and enrichment schemes for finite element and finite sphere discretizations. Comput Struct 2005;83:1386–95.
[27] Liu GR. Meshfree methods – moving beyond the finite element methods. 2nd ed. CRC Press; 2009.
[28] Oñate E, Idelsohn S, Zienkiewicz OC, Taylor RL. A finite point method in computational mechanics – applications to convective transport and fluid flow. Int J Numer Methods Eng 1996;39:3839–66.
[29] Shi GH. Manifold method of material analysis. In: Transactions of the 9th army conference on applied mathematics and computing, Report No. 92-1, US Army Research, Office, 1991.
[30] Shi GH. Manifold method. In: Proceedings of the first international forum on discontinuous deformation analysis (DDA) and simulations of discontinuous media, New Mexico, USA, 1996, p. 52–204.
[31] Shi GH. Numerical manifold method. In: Proceedings of the 2nd international conference on analysis of discontinuous deformation, Kyoto, Japan, 1997, p. 1–35.
[32] Shi GH. Application of discontinuous deformation analysis and manifold method. In: Proceedings of ICADD-3, third international conference on analysis of discontinuous deformation from theory to practice. Colorado: American Rock Mechanics Association; 1999. p. 3–16.
[33] Shi GH. Block system modeling by discontinuous deformation analysis. Southampton, UK: Computational Mechanics Publications; 1993.
[34] Liu J, Kong X, Lin G. Formulations of the three-dimensional discontinuous deformation analysis method. Acta Mech Sin 2004;20:270–82.
[35] Grayeli R, Mortazavi A. Discontinuous deformation analysis with second-order finite element meshed block. Int J Numer Anal Methods Geomech 2006;30:1545–61.

[36] Ma G, An X, Zhang H, Li L. Modeling complex crack problems using the numerical manifold method. Int J Fract 2009;156:21–35.
[37] Zhang H, Li L, An X, Ma G. Numerical analysis of 2-D crack propagation problems using the numerical manifold method. Eng Anal Bound Elem 2010;34:41–50.
[38] Ning Y, An X, Ma G. Footwall slope stability analysis with the numerical manifold method. Int J Rock Mech. Min. Sci. 2011;48:964–75.
[39] Ham S, Bathe KJ. A finite element method enriched for wave propagation problems. Comput Struct 2012;94–95:1–12.
[40] An X, Li L, Ma G, Zhang H. Prediction of rank deficiency in partition of unity-based methods with plane triangular or quadrilateral meshes. Comput Methods Appl Mech Eng 2011;200:665–74.
[41] Chen G, Ohnishi Y, Ito T. Development of high-order manifold method. Int J Numer Methods Eng 1998;43:685–712.
[42] Cheng YM, Zhang YH, Chen WS. Wilson non-conforming element in numerical manifold method. Commun Numer Methods Eng 2002;18:877–84.
[43] Zhang G, Sigiura Y, Hasegawa H, Wang G. The second order manifold method with six node triangle mesh. Struct Eng/Earthq Eng JSCE 2002;19:1–9.
[44] Li S, Cheng Y, Wu Y-F. Numerical manifold method based on the method of weighted residuals. Comput Mech 2005;35:470–80.
[45] He L, Ma G. Development of 3D numerical manifold method. Int J Comput Methods 2010;7:107–29.
[46] Ma G, An X, He L. The numerical manifold method: a review. Int J Comput Methods 2010;7:1–32.
[47] Okazawa S, Terasawa H, Kurumatani M, Terada K, Kashiyama K. Eulerian finite cover method for solid dynamics. Int J Comput Methods 2010;7:33–54.
[48] Xuli H. Multi-node higher order expansions of a function. J Approx Theor 2003;124:242–53.
[49] Guessab A, Nouisser O, Schmeisser G. Multivariate approximation by a combination of modified Taylor polynomials. J Comput Appl Math 2006;196:162–79.
[50] Zuppa C. Modified Taylor reproducing formulas and h-p clouds. Math Comput 2008;77(261):243–64.
[51] Oden JT, Duarte CA, Zienkiewicz OC. A new cloud-based hp finite element method. Comput Methods Appl Mech Eng 1998;153:117–26.
[52] Duarte CA, Babuška I, Oden JT. Generalized finite element methods for three-dimensional structural mechanics problems. Comput Struct 2000;77:215–32.
[53] Pereira JP, Duarte CA, Guoy D, Jiao X. *Hp*-Generalized FEM and crack surface representation for non-planar 3-D cracks. Int J Numer Methods Eng 2009;77:601–33.
[54] Tian R, Yagawa G, Terasaka H. Linear dependence problems of partition of unity-based generalized FEMs. Comput Methods Appl Mech Eng 2006;195:4768–82.
[55] Bucalem ML, Bathe KJ. The mechanics of solids and structures – hierarchical modeling and the finite element solution. Springer; 2011.
[56] Payen DJ, Bathe KJ. Improved stresses for the 4-node tetrahedral element. Comput Struct 2011;89:1265–73.
[57] Payen DJ, Bathe KJ. A stress improvement procedure. Comput Struct 2012;112-113:311–26.
[58] Chapelle D, Bathe KJ. The finite element analysis of shells – fundamentals. 2nd ed. Springer; 2011.
[59] Bathe KJ, Lee PS. Measuring the convergence behavior of shell analysis schemes. Comput Struct 2011;89:285–301.